

Short Communication

Synthesis of Monodispersed Pt-Ni Alloy Nanodendrites and Their Electrochemical Properties

Young-Woo Lee¹, Bo-Young Kim¹, Kyung-Hoon Lee¹, Woo-Jin Song¹, Guozhong Cao²,
Kyung-Won Park^{1,*}

¹ Department of Chemical Engineering, Soongsil University, Seoul 156-743, Republic of Korea

² Department of Materials Science and Engineering, University of Washington, Seattle, WA 98195, USA

*E-mail: kwpark@ssu.ac.kr

Received: 17 December 2012 / Accepted: 9 January 2013 / Published: 1 February 2013

Structure-controlled Pt-based catalysts have been known to exhibit improved electrocatalytic activities due to particularly modulated surface structures favorable for alcohol electrooxidation. We report Pt-Ni alloy dendrite structure for formic acid electrooxidation prepared by a thermal decomposition method. The Pt-Ni nanodendrites display 3-dimensional nanostructure and homogeneous alloy formation between Pt and Ni. In formic acid electrooxidation, the Pt-Ni alloy nanodendrite catalyst exhibits much improved electrocatalytic activity.

Keywords: Platinum, Nickel, Alloy, Dendrites, Formic acid, Electrooxidation

1. INTRODUCTION

Noble metallic nanoparticles (NPs) have received extensive interests due to their particular electrochemical, photochemical, biochemical, sensor, and catalytic properties [1-5]. The shape-controlled metal NPs have been synthesized with 0-dimensional (cube, octahedron, truncated cube, and tetrahedron, etc.) [6-10], 1-dimensional (nanowire, nanorod, and nanotube, etc.) [11-13], 2-dimensional (nanoplate and nanosheet, etc.), and 3-dimensional (nanostar, nanoflower, and nanodendrite, etc.) structures [14-17]. In recent, it has been reported that shape-controlled NPs exhibits much improved thermal, chemical, magnetic, electronic, and catalytic properties as compared to bulk structure.

In particular, dendritic and flower-like nanostructures for electrochemical power sources have shown much enhanced electrocatalytic activity and stability [18]. To improve the electrocatalytic properties of metallic nanostructure catalysts, there have been many efforts to manipulate the structure

and shape of NPs during the synthetic process. The metallic nanostructures can have significantly enhanced catalytic reaction rates over those of bulk materials. Xia *et al.*, Wang *et al.*, and Yang *et al.* reported that Pt-based nanostructure catalysts exhibit improved methanol electrooxidation and oxygen reduction reaction due to high-index facets such as {311}, {730}, and {830}, and high surface area of dendritic structures [18-20]. Furthermore, it is likely that the nanodendritic structures of Pt-based alloy electrocatalysts can have many merits in electrochemical applications. Accordingly, the crucial factors affecting catalytic properties in metallic electrocatalysts for fuel cell applications might be the structure and shape of catalysts.

A variety of shape-controlled metallic NPs have been successfully prepared by means of chemical, thermal, electrochemical, and photochemical reduction methods [21-24]. Among them, the thermal decomposition method is suitable for the synthesis of structure-controlled noble metallic NPs with homogeneous size and shape [25-27]. Herein, we synthesized Pt-Ni alloy nanodendrites for formic acid electrooxidation by using thermal decomposition method. The structure and composition of the Pt-Ni alloy nanodendrites were characterized by field-emission transmission electron microscopy (FE-TEM), energy dispersive X-ray (EDX) spectroscopy, and X-ray diffraction (XRD). The electrocatalytic properties of the alloy nanodendrites were measured and compared using a potentiostat.

2. EXPERIMENTAL PART

2.1. Synthesis of Pt-Ni alloy nanodendrites

The Pt-Ni alloy nanodendrites were prepared by reducing Pt and Ni salt in organic-based solution. All chemicals used were of analytical grade. For solution of dissolved Platinum acetylacetonate (Pt(acac)₂, Aldrich) and Nickel acetylacetonate (Ni(acac)₂, Aldrich) salt, the 5 mL 1-octadecene (C₁₈H₃₆, Aldrich) and 4.22 mL oleyamine (C₁₈H₃₇N, Aldrich) solution containing 4.5 mM Pt(acac)₂ and 1.5 mM Ni(acac)₂ was prepared in a 30 mL vial. For perfect dissolution of Pt and Ni salt, the mixture solution were dissolved with continuous stirring and kept for 30 min at 70 °C. On the other hand, the 10.78 mL 1-octadecene and 5 mL oleyamine solution containing 50.4 mg oxalic acid (C₂H₂O₄·2H₂O, Johnson Matthey Co.) was prepared in a three-neck flask (50 mL) under a nitrogen atmosphere. The mixed solutions were raised by 7 °C min⁻¹ and kept for 1 h at 250 °C. The dissolved Pt and Ni salt solution was injected into heating solvent with continuous stirring and kept for 2 h at 250 °C until Pt and Ni salts were completely reduced under nitrogen atmosphere. The resulting colloid solution was rapidly cooled into hexane and black colloid was observed indicating the formation of Pt-Ni alloy nanoparticles.

2.2 Preparation of Pt-Ni alloy nanodendrites deposited on carbon black

The carbon (Vulcan XC-72R) powder was stirred in 5 M HCl solution at 50 °C for 12 h and then washed with water and ethanol several times to remove impurity and HCl. The 50 mL colloid

solution containing as-synthesized Pt-Ni alloy nanodendrites (24.1 mg) was putted to 30 mL of acetic acid (2 M) and 20 mL acetone for well-depositd Pt-Ni alloy nanodendrites on carbon black and removed the organic materials. The Vulcan XC-72R (96.4 mg) as supports were added to the solution and mixed with continuous stirring at room temperature for 24 h. The resulting powder was precipitated and washed with acetone, ethanol, and water to remove surfactant and impurity.

2.3. Structural analysis

For the structure analysis of the catalysts, X-ray diffraction (XRD) analysis was carried out using a Rigaku X-ray diffractometer with Cu K_{α} ($\lambda = 0.15418$ nm) source with a Ni filter. The source was operated at 40 kV and 100 mA. The 2θ angular scan from 20° to 80° was explored at a scan rate of $3^{\circ} \text{ min}^{-1}$. For all the XRD measurement, the resolution in the scans was kept at 0.02° . The morphology and size distribution of the catalysts were characterized by field-emission transmission electron microscopy (TEM) using a Tecnai G2 F30 system operating at 300 kV. TEM samples were prepared by placing drops of catalyst suspension dispersed in ethanol on a carbon-coated copper grid. Energy dispersive X-ray (EDX) analysis of the catalysts was performed on a field emission transmission electron microscope (FE-TEM, Tecnai G2 F30 system).

2.4 Electrochemical analysis

Electrochemical properties of the catalysts were measured in a three-electrode cell at 25°C using a potentiostat (CH Instrument, CHI 700C). A Pt wire and Ag/AgCl (in saturated KCl) were used as a counter and reference electrode, respectively. The catalyst ink was prepared by ultrasonically dispersing catalyst powders in an appropriate amount of Millipore water and 5 wt% Nafion[®] solution (Aldrich). The catalyst ink was prepared by mixing 2 mg metal of all catalysts, 150 μL of Millipore water, 57.2 μL of 5 wt% Nafion[®] solution, and 500 μL of 2-propanol solution ($\text{C}_3\text{H}_8\text{O}$, Sigma). The catalyst ink was dropped onto a glassy carbon working electrode (area $\sim 0.0706 \text{ cm}^2$). After drying in 50°C oven, total loading of catalyst was $20 \mu\text{g cm}^{-2}$. To evaluate electrocatalytic activities of the as-prepared catalysts, CVs were obtained between -0.2 to $+1.0$ V in Ar-saturated $0.1 \text{ M HClO}_4 + 2 \text{ M HCOOH}$ with a scan rate of 50 mV s^{-1} at 25°C . The electrochemical active surface areas (EASAs) of the Pt catalysts were measured by integrating hydrogen desorption regions (assuming $210 \mu\text{C cm}^{-2}$ of a polycrystalline Pt electrode) in 0.1 M HClO_4 solution.

3. RESULTS AND DISCUSSION

The structure analysis of the as-synthesized Pt-Ni NPs was carried out by FE-TEM. The Pt-Ni NPs exhibit fairly uniform dendritic shape as indicated in Fig. 1(a). As shown in high-resolution TEM (HR-TEM) images of Fig. 1(b), it is observed that the Pt-Ni nanodendrites are grown along multi-pod nanostructure. Furthermore, in Fig. 1(c), a line scanning profile across a Pt-Ni nanodendites by energy

dispersive X-ray (EDX) spectroscopy shows a homogenous distribution of both platinum and nickel in the dendritic shape. As confirmed by the EDX, the Pt-Ni nanodendrites are alloy particles containing 73.6 at% of Pt and 26.4 at% of Ni. This represents that the Pt-Ni nanodendrites are homogeneous alloy structure consisting of platinum and nickel in the dendritic NPs, prepared by complete reduction of metal salts for an intentional ratio of platinum to nickel. The average size of the Pt-Ni alloy nanodendrites are ~ 21.7 nm in Fig. 1(d).

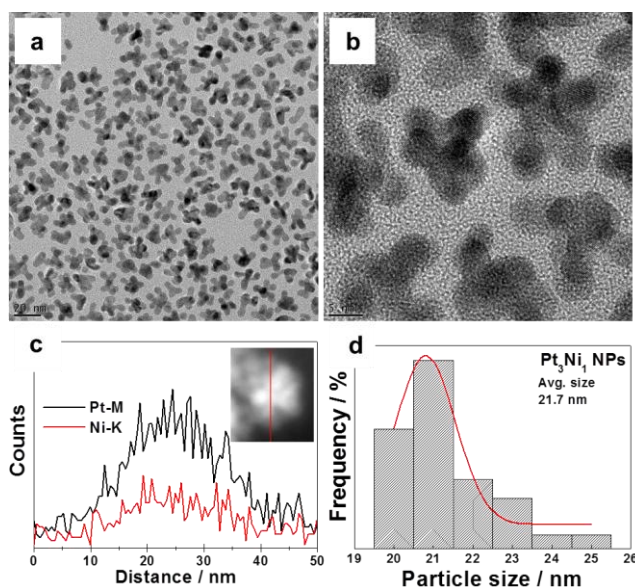


Figure 1. (a) FE-TEM and (b) HR-TEM image of the Pt-Ni alloy nanodendrites. (c) A line scanning profile across a Pt-Ni nanodendrites. (d) Particle size distribution of the Pt-Ni alloy nanodendrites.

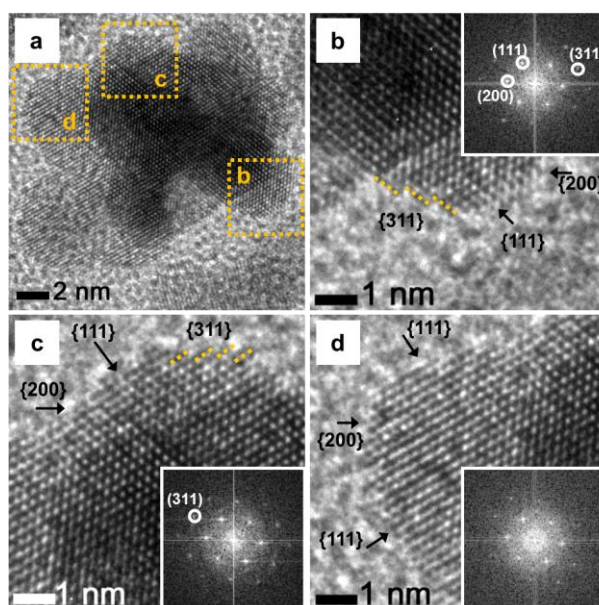


Figure 2. (a) A HR-TEM and (b-d) HR-TEM images of nanobranches in the Pt-Ni alloy nanodendrite. The insets indicate the FFT patterns of the Pt-Ni alloy nanodendrites.

Fig. 2(a) displays a HR-TEM image of a Pt-Ni alloy nanodendrite grown with multi-branches. As indicated in Fig. 2(b-d), the individual Pt-Ni alloy nanobranches appear crystalline structures with highly ordered branches. The exposed nanobranches consist of {111}, {200} and high-index {311} facets. The corresponding fast Fourier transform (FFT) patterns (the insets of the Fig. 2(b-d)) represent that the Pt-Ni alloy nanobranches are single nanocrystals enclosed by {111}, {200}, and {311} facets. Interestingly, the nanostructure catalysts with high-index facets such as {311} have exhibited much improved electrocatalytic activity and stability in electrochemical power sources [28]. Thus, it is expected that the Pt-Ni alloy nanodendrites can show much improved electrocatalytic properties in formic acid electrooxidation.

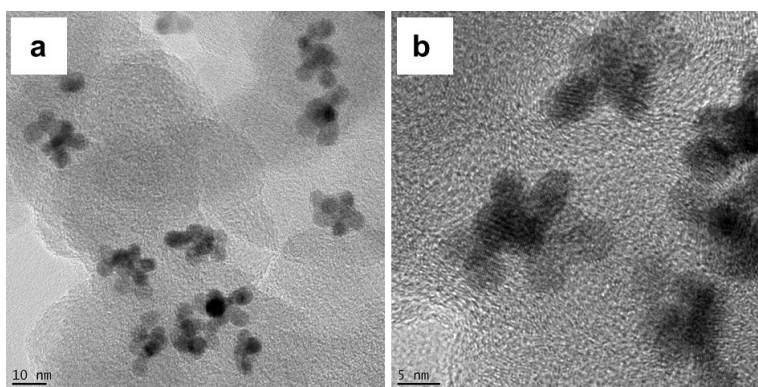


Figure 3. (a) FE-TEM and (b) HR-TEM images of Pt-Ni alloy nanodendrites deposited on carbon black (Vulcan XC-72R).

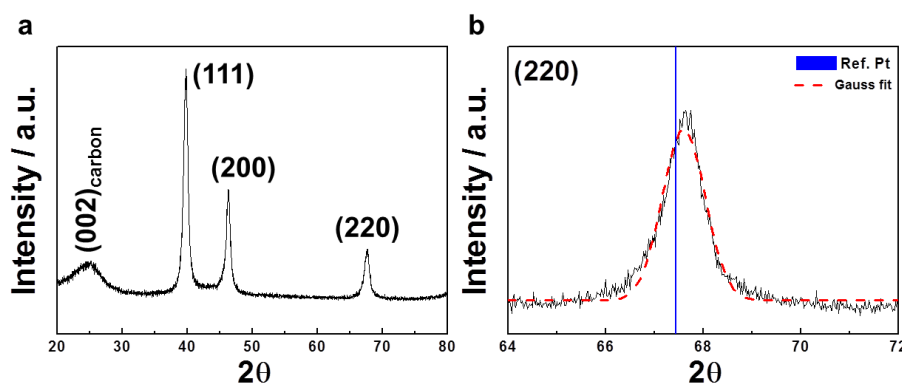
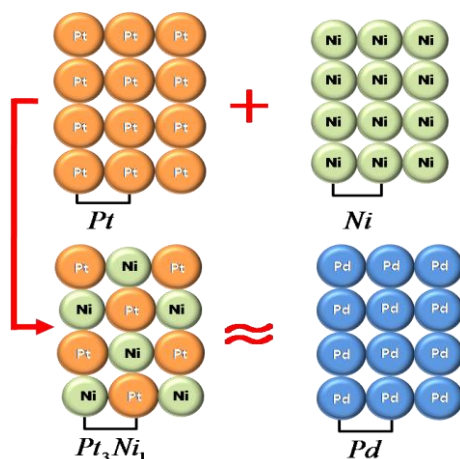


Figure 4. (a) The Wide-range XRD patterns and (b) the diffraction peak of (220) plane of D-Pt-Ni/C.

For electrochemical analysis, we prepared the Pt-Ni alloy nanodendrites deposited on carbon black (denoted as D-Pt-Ni/C). As shown in Fig. 3, the Pt-Ni alloy nanodendrite catalysts are well dispersed on carbon support (Vulcan XC-72R). The Pt-Ni alloy nanodendrites appear no aggregation or etching during deposited process. The XRD peaks of the D-Pt-Ni/C at 39.804° , 46.329° , and 67.654° correspond to (111), (200) and (220), respectively, of a face centered cubic (fcc) crystal structure (Fig. 4(a)). The broad peak at around 25° is associated with (002) plane of the carbon black. In the case of

(220) plane of the D-Pt-Ni/C, the diffraction peak shows an evident positive angle shift of $\sim 0.2^\circ$ in comparison with reference data of Pt (JCPDS No. 04-0802) (Fig. 4(b)). The positive angle shift in the XRD peak of the D-Pt-Ni/C reflects well-defined alloy formation between Pt and Ni in the Pt-Ni dendrite nanostructure catalyst [29].



Scheme 1. Relationship of lattice parameters of Pt, Ni, Pd, and Pt_3Ni_1 .

The Pt- or Pd-based catalysts for electrooxidation reaction of formic acid have exhibited the enhanced electrochemical properties such as lower on-set potential and higher current density than other catalysts [30,31]. Recently, Osawa *et al.* observed the role of the bridge-bonded adsorbed formate in the electrocatalytic oxidation of formic acid on catalyst surface using time-resolved surface-enhanced infrared absorption spectroscopy [32-34].

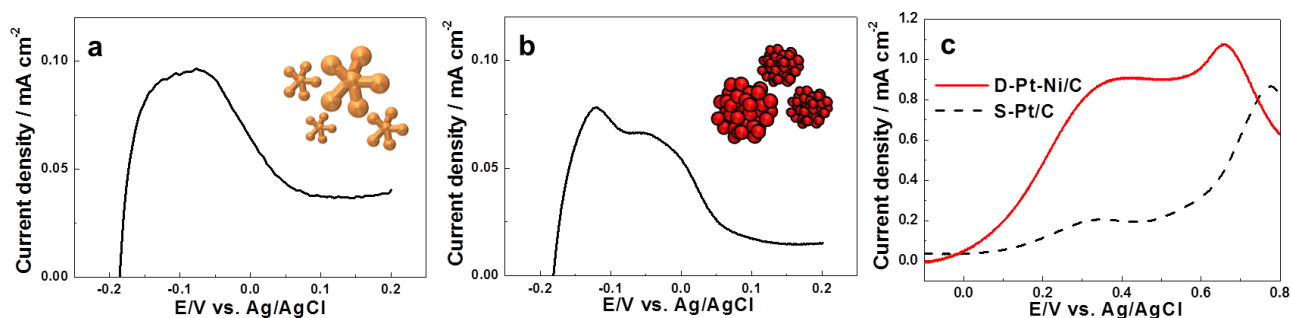
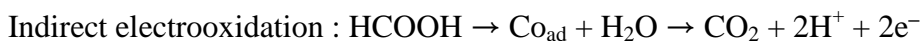


Figure 5. Voltammograms of (a) D-Pt-Ni/C and (b) S-Pt/C in 0.1 M $HClO_4$ with a scan rate of 50 mV s^{-1} at 25°C . (c) CVs of D-Pt-Ni/C and S-Pt/C in 0.1 M $HClO_4$ + 0.2 M formic acid with a scan rate of 50 mV s^{-1} . The loading amount of metal catalyst on the electrode is $20 \mu\text{g cm}^{-2}$.

In particular, the major key for an enhanced electrocatalytic activity is surface structure or lattice parameter of catalysts because of bridge-bonded adsorption of formate during oxidation reaction of formic acid on catalyst surface. Scheme 1 shows correlation between Pt-Ni alloy and pure Pd as a function of lattice parameters of metals. The lattice parameter of pure Pt (3.939 \AA) is larger than that of

pure Pd (3.893 Å). If Pt atoms are alloyed with metal atoms of smaller size, the lattice parameter of the Pt-based alloy is reduced and similar to that of pure Pd. Herein, we selected Ni (3.523 Å) having an fcc structure as a 2nd metal for the control of surface structure. As already confirmed in XRD data, the lattice parameter of Pt₃Ni₁ alloy (3.898 Å) is similar to that of pure Pd. Thus, it is expected that the as-prepared Pt₃Ni₁ alloy nanodendrites can exhibit improved electrocatalytic properties in formic acid oxidation reaction in comparison with pure Pt.

To identify electrochemical properties of the catalysts, cyclic voltammograms (CVs) were obtained in 0.1 M HClO₄ in Fig. 5(a and b). The voltammograms of the as-prepared catalysts for formic acid electrooxidation are shown in Fig. 5(c). In the voltammograms, the D-Pt-Ni/C indicates much lower onset potential than spherical Pt/C (denoted as S-Pt/C (E-TEK, Co.)). Furthermore, the D-Pt-Ni/C exhibits the more negative peak potential than the S-Pt/C. In the formic acid electrooxidation on Pt surface, two oxidation peaks appear at ~0.30 and ~0.70 V during the positive potential scan between -0.1 and 0.8 V. The formic acid electrooxidation on Pt-based catalysts has been widely investigated as a model of electrocatalytic reactions. The reaction mechanism of the formic acid electrooxidation is typically described by direct or step pathway. The first anodic peak at around 0.3 V corresponds to direct electrooxidation of formic acid to CO₂, which is greatly affected by the poisoning of the electrode surface due to the adsorption of the reaction intermediate (CO_{ad}). The second anodic peak at 0.70 V corresponds to the oxidation of the CO_{ad} generated during the dissociative adsorption step [33,35].



The D-Pt-Ni/C shows an improved 1st anodic current density (0.905 mA cm⁻²) in comparison with the S-Pt/C (0.208 mA cm⁻²). The ratio of 1st to 2nd anodic current density of the D-Pt-Ni/C is 3.51 times higher than that of the S-Pt/C. It is likely that the improved electrochemical properties of the D-Pt-Ni/C can result from alloy formation favorable to the electrooxidation and nanostructure with high-index facet. Thus, it is expected that the D-Pt-Ni/C may be a promising anode catalyst for formic acid electrooxidation based on acidic electrolyte.

4. CONCLUSIONS

We have synthesized Pt-Ni alloy nanodendritic catalyst for formic acid electrooxidation by a thermal decomposition method. The as-synthesized Pt-Ni alloy catalyst exhibited 3-dimensional dendritic structure with fairly uniform particle size and shape. The lattice parameter of the Pt-Ni catalyst similar to that of pure Pd could be controlled. In the formic acid electrooxidation, the Pt-Ni dendritic catalyst with high-index facet and well-defined alloy formation between Pt and Ni showed highly improved electrocatalytic properties.

ACKNOWLEDGMENTS

This work was supported by the National Research Foundation of Korea Grant funded by the Korean Government (NRF- 2011-0030335).

References

1. I.-T. Kim, H.-K. Lee and J. Shim, *J. Nanosci. Nanotech.*, 8 (2008) 5302.
2. S.-W. Xie, S. Chen, Z.-Q. Liu and C.-W. Xu, *Int. J. Electrochem. Sci.*, 6 (2011) 882.
3. S. Lj. Gojković, T. R. Vidaković and D. R. Durović, *Electrochim. Acta*, 48 (2003) 3607.
4. J. M. S. Ayub, R. F. B. De Souza, J. C. M. Silva, R. M. Piasentin, E. V. Spinacé, M. C. Santos and A. O. Neto, *Int. J. Electrochem. Sci.*, 7 (2012) 11351.
5. M. D. Obradović and S. Lj. Gojković, *J. Electroanal. Chem.*, 664 (2012) 152.
6. Y. W. Lee, M. Kim and S. W. Han, *Chem. Commun.*, 46 (2010) 1535.
7. Y. Kang, X. Ye and C. B. Murray, *Angew. Chem. Int. Ed.*, 49 (2010) 6156.
8. Y.-W. Lee, A.-R. Ko, S.-B. Han, H.-S. Kim, D.-Y. Kim, S.-J. Kim and K.-W. Park, *Chem. Commun.*, 46 (2010) 9241.
9. Y.-W. Lee, A.-R. Ko, S.-B. Han, H.-S. Kim and K.-W. Park, *Phys. Chem. Chem. Phys.*, 13 (2011) 5569.
10. Y.-W. Lee, S.-B. Han, A.-R. Ko, H.-S. Kim and K.-W. Park, *Catal. Commun.*, 15 (2011) 137.
11. D. Seo and H. Song, *J. Am. Chem. Soc.*, 131 (2009) 18210.
12. L. Wang and Y. Yamauchi, *J. Am. Chem. Soc.*, 132 (2010) 13636.
13. Z. Chen, M. Waje, W. Li and Y. Yan, *Angew. Chem. Int. Ed.*, 46 (2007) 4060.
14. A. Mohanty, N. Garg and R. Jin, *Angew. Chem. Int. Ed.*, 49 (2010) 4962.
15. B. Lim, M. Jiang, T. Yu, P. H. C. Camargo and Y. Xia, *Nano Res.*, 3 (2010) 69.
16. L. Wang, Y. Nemoto and Y. Yamamuchi, *J. Am. Chem. Soc.*, 133 (2011) 9674.
17. L. Wang and Y. Yamauchi, *J. Am. Chem. Soc.*, 131 (2009) 9152.
18. Z. Peng and H. Yang, *J. Am. Chem. Soc.*, 131 (2009) 7542.
19. B. Lim, M. Jiang, P. H. C. Camargo, E. C. Cho, J. Tao, X. Lu and Y. Xia, *Science*, 324 (2009) 1302.
20. N. Tian, Z.-Y. Zhou, S.-G. Sun, Y. Ding and Z. L. Wang, *Science*, 316 (2007) 732.
21. S.-I. Choi, R. Choi, S. W. Han and J. T. Park, *Chem. Commun.*, 46 (2010) 4950.
22. Q. Zhang, J. Xie, J. Liang and J. Y. Lee, *Adv. Funct. Mater.*, 19 (2009) 1387.
23. H. Lee, S. E. Habas, S. KweSkin, D. Butcher, G. A. Somorjai and P. Yang, *Angew. Chem. Int. Ed.*, 45 (2006) 7824.
24. Y.-W. Lee, J.-K. Oh, H.-S. Kim, J.-K. Lee, S.-B. Han, W. Choi and K.-W. Park, *J. Power Sources*, 195 (2010) 5896.
25. M. Subramannia and V.K. Pillai, *J. Mater. Chem.*, 18 (2008) 5858.
26. Y. Bing, H. Liu, L. Zhang, D. Ghosh and J. Zhang, *Chem. Soc. Rev.*, 39 (2010) 2184.
27. Y.-W. Lee, S.-B. Han, D.-Y. Kim and K.-W. Park, *Chem. Commun.*, 47 (2011) 6296.
28. M. Jin, H. Zhang, Z. Xie and Y. Xia, *Angew. Chem. Int. Ed.*, 50 (2011) 7850.
29. Y. Yamauchi, S. S. Nair, T. Momma, T. Ohsuna, T. Osaka and K. Kuroda, *J. Mater. Chem.*, 16 (2006) 2229.
30. Z. Liu, L. Hong, M. P. Tham, T. H. Lim and H. Jiang, *J. Power Sources*, 161 (2006) 831.
31. H. Li, G. Sun, Q. Jiang, M. Zhu, S. Sun and Q. Xin, *Electrochem. Commun.*, 9 (2007) 1410.
32. M. Osawa, K. Komatsu, G. Samjeské, T. Uchida, T. Ikeshoji, A. Cuesta and C. Gutiérrez, *Angew. Chem. Int. Ed.*, 50 (2011) 1159.
33. A. Miki, S. Ye and M. Osawa, *Chem. Commun.*, (2002) 1500.
34. Y. Shen, G. Lu, Y. Guo, Y. Wang, Y. Guo and X. Gong, *Catal. Today*, 175 (2011) 558.
35. J. Masud, M. T. Alam, M. R. Miah, T. Okajima and T. Ohsaka, *Electrochem. Commun.*, 13 (2011) 86.